Target and projectile fragmentations in ^{208}Pb-emulsion collisions at 160*A* GeV

G. Singh and P. L. Jain
High Energy Experimental Laboratory, Department of Physics, State University of New York at Buffalo, Buffalo, New York 14260
(Received 20 February 1996)

We present the results of a study performed on the ^{208}Pb-emulsion interactions at 160*A* GeV. In a minimum-bias sample of 1034 nuclear collisions, charges are assigned to all of the emitted 3431 helium and 1820 heavier projectile fragments during the breakup of the ^{208}Pb beam in emulsion. Multiplicity distributions of the target-associated slow-moving particles and of the fast-moving projectile fragments are investigated. The polar angles of a subsample of 337 interactions having at least four projectile fragments of charge $Z \geqslant 2$ are accurately measured and their pseudorapidity distributions are obtained. Multiplicity distributions, two- and three-body asymmetries, and conditional moments of the fast-moving projectile particles are investigated in terms of the total charge remaining in bound in the multiply charged projectile fragments. The results are compared with our existing 10.6*A* GeV ^{197}Au-emulsion data obtained in experiment No. 875 conducted at the Brookhaven National Laboratory. Multiplicity distributions of slow particles emitted from the ^{208}Pb- and ^{197}Au-induced emulsion reactions are found to be independent of the beam masses and their energies. An insignificant number of fission events is observed in this work. Some differences in the average yields of helium nuclei and heavier fragments are observed, which may be attributed to an energy effect or to the limited statistics. However, two- and three-body asymmetries and conditional moments indicate that the breakup mechanism of the projectiles over a wide span of energies seems to be energy independent. [S0556-2813(96)01012-6]

PACS number(s): 25.75.−q, 05.70.Jk, 24.60.Ky, 25.70.Pq

I. INTRODUCTION

The collisions of heavy ions at relativistic energies offer the right kind of environment to explore a variety of aspects related to hot and dense nuclear matter to enhance our existing knowledge about the nuclear equation of state (EOS), as well as the possibility of observing the signatures of an unusual form of matter such as a quark-gluon plasma. Thus, an intensive effort has been devoted, during recent years, to investigate the formation and decay of highly excited nuclear matter produced in nucleus-nucleus collisions at various incident energies. Depending upon the target-projectile combination and the incoming projectile energy, the excited piece of nuclear matter decays predominantly by the emission of nucleons, deuterons, tritons, helium nuclei, and charged particles with $3 \leqslant Z \leqslant 30$ commonly known as intermediate-mass fragments (IMF's) and fragments of very heavy charge $Z > 31$. To understand the dynamics involving the formation of IMF's and other multifragments in its final state, numerous experiments have been performed at low, intermediate, and high energies [1–5]. To explain the experimental results on the still debated subject of nuclear multifragmentation, several alternative theoretical approaches [6,7] have been put forward in which the formation and decay of IMF's are assumed to take place through the statistically fragmenting processes or through the dynamical processes such as the Boltzmann-Uehling-Uhlenbeck formalism [8], the microscopic quantum molecular dynamics (QMD) calculations [9], and the role of mass and energy density fluctuations in the phenomena of cluster formation [10]. Thus, more experimental information is clearly required in order to disentangle various existing models on this interesting topic of multifragmentation.

Very recently, a beam of ^{208}Pb nuclei has been accelerated to an energy of 160*A* GeV from the CERN Super Proton Synchrotron (SPS). Consequently, it has provided an ample opportunity to investigate the formation and decay of highly excited nuclear matter under the conditions of extreme density and temperature. In the following discussion, we shall present, *for the first time*, a systematic study on the target and the projectile fragmentations of the ^{208}Pb-induced emulsion interactions at the highest available projectile energy of $\approx$33 TeV from the SPS accelerator facility. An attempt is also made to compare these results with our data [3] collected on the ^{197}Au beam at 10.6*A* GeV from the BNL Alternating Gradient Synchrotron (AGS).

This paper is organized as follows. In Sec. II, we give the experimental details that include the exposure and scanning of emulsion stacks, different kinds of the produced particles, and the charge determination of the fast-moving projectile fragments. The discussion of the results of the slow-moving target-related particles is given in Sec. III, and that of the fast moving projectile fragments (PF's) of charge $Z \geqslant 2$ in Sec. IV. Section V deals with the discussion pertaining to the two- and three-body asymmetries of the fast-moving charged particles, and Sec. VI presents their conditional moments in terms of the bound charge Z_{bound} [2]. Finally, the conclusions of the present experiment are reported in Sec. VII.

II. EXPERIMENTAL DETAILS

A. Exposure and scanning of emulsion stacks

In December 1994, three stacks, each one consisting of 16 electron-sensitive Fuji nuclear emulsions, were exposed to a beam of ^{208}Pb ions at 160*A* GeV in experiment. No. EMU11 conducted at the CERN SPS. The flux of the incoming ^{208}Pb beam was 1000 ions/cm^2. The exposure was made in such a way that these energetic ^{208}Pb nuclei remained almost parallel to the surface of an emulsion pellicle. Thus, the in-

dividual beam tracks were, in general, confined to a single pellicle and the following of the primary beam tracks was done only in one emulsion plate. By employing along-the-track scanning technique under a total magnification of $\approx 550\times$, we followed all of the primary tracks of the ^{208}Pb beam initiating from the entrance edge until they either interacted or exited from the interacting volume. By following a total track length of 58.29 m, a data sample of 1300 nuclear interactions was collected and is considered as the minimum-bias sample for the present experiment. The nuclear interaction mean-free-path value determined in the present experiment is $\lambda_{\rm nuc}=4.48\pm 0.12$ cm and the corresponding value of its nuclear cross section in emulsion is $\sigma_{\rm nuc}=2826\pm 78$ mb [11]. For the present investigation, 1034 nuclear events have been completely analyzed and discussed. The results are compared with another sample of 1224 ^{197}Au-emulsion collisions at 10.6A GeV obtained through experiment No. 875 performed at the BNL AGS [3].

B. Classification of emitted particles

In general, four kinds of charged particles are observed in the interactions of heavy ions in emulsions: (i) the target-associated slow-moving particles emitted from the excitation of an emulsion target nucleus, (ii) the fast-moving projectile fragments of charge $Z\geqslant 2$, (iii) the projectile fragments of charge $Z=1$ emitted from the fragmentation of the ^{208}Pb beam nucleus, and (iv) the singly charged produced particles (predominantly π mesons). At the SPS relativistic energies, first and second classes of particles can be easily distinguished from their visual characteristics in nuclear emulsions [11,12]. A great majority of the target-associated particles have relatively low energies. In the conventional terminology of emulsions [11], these particles are known as black, N_b, and grey, N_g, tracks. N_b tracks are charged particles having a velocity $v\leqslant 0.2c$ with a residual range of $R<3$ mm in emulsion. Generally, N_b tracks are due to protons of kinetic energy, $E_k<20$ MeV, and are the fragments evaporated from the target. Some black tracks are also due to the helium and heavier charges [11]. N_g particles have a velocity $0.2c<v<0.7c$ with a residual range of $R\geqslant 3$ mm. These particles predominantly comprise of protons of kinetic energy between $26\leqslant E_k\leqslant 375$ MeV and occasionally kaons between $20\leqslant E_k\leqslant 198$ MeV and π mesons between $12\leqslant E_k\leqslant 56$ MeV [11]. The multiplicity of heavy tracks, N_h, is generally defined as $N_h=N_b+N_g$. At relativistic energies, multiply charged fragments with $Z\geqslant 2$ emitted from the breakup of the projectile nucleus essentially travel with the same speed as that of the parent beam nucleus. These energetic PF's are recorded in emulsion with 100% detection efficiency and this intrinsic feature of emulsion makes it a unique detector among all the particle detectors currently in use. In each event, we recorded the multiplicity of helium tracks, N_α, as well as of the projectile fragments with $Z\geqslant 3$, $N_{\rm PF}$. However, for the third and fourth categories of particles, it is difficult to make a clear distinction, especially between the singly charged PF's and the singly charged produced π mesons proceeding in the very forward direction. These particles produce minimum ionizing tracks in emulsion and hence they look alike. In addition, some of the singly charged PF's can participate during the collision and

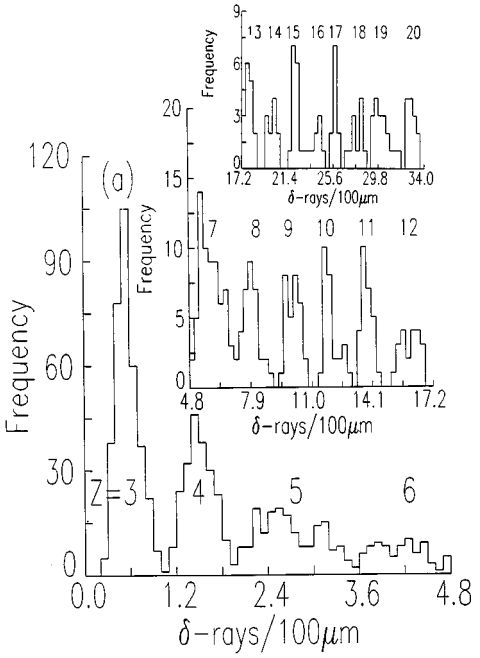

FIG. 1. Frequency distribution of δ rays per 100 μm of the PF's of charge $3\leqslant Z\leqslant 20$ in nuclear events of ^{208}Pb at 160A GeV.

can mix with the produced π mesons emitted at large angles, and thus their separation is not easy. Dealing with massive ions like ^{208}Pb and ^{197}Au at very high energies, there is another possibility that some of the target protons are knocked out by the incident projectile nucleus and appear as fast-moving particles, which are hard to distinguish from the singly charged projectile fragments. However, the number of singly charged projectile fragments, in general, can be determined from the charge conservation using Eq. (1) as described in Sec. IV B.

C. Charge determination of projectile fragments

The grain density of singly charged relativistic tracks ($Z=1$) was determined to be 25–30 grains/(100 μm). The grain density of the relativistic helium tracks (with $Z=2$) was almost 4 times than that of the minimum ionizing tracks, and thus the helium tracks were easily recognized by an experienced observer due to their distinctive grain density. Furthermore, all the helium track candidates were followed for more than 5 cm to ensure that they might not be due to some grey tracks proceeding downstream in the very forward direction. Almost 99% of the grey tracks when followed up to 5 cm showed a considerable amount of Coulomb scattering and, with further tracing, they came to the end of their ranges, but not the projectile helium tracks. The charges of all the PF's with $Z\geqslant 3$ were determined by a combination of several methods: grain density, gap length, δ-ray density, relative track width, etc., as discussed in our former investigation [3]. In Fig. 1, we present the frequency distribution of (δ rays)/(100 μm) for the PF's of charge $3\leqslant Z\leqslant 20$. For δ-ray density, more than 200 δ-rays were counted for each track. A well-defined peak corresponding to each individual charge is an indication of very good charge resolution achieved up to $Z=20$. The charge resolutions obtained for the charge groups $2\leqslant Z\leqslant 4$, $5\leqslant Z\leqslant 12$, $13\leqslant Z\leqslant 20$,

TABLE I. The average multiplicity of target-associated black $\langle N_b \rangle$, grey $\langle N_g \rangle$, and heavy $\langle N_h \rangle$ particles emitted in the ^{208}Pb- and ^{197}Au-induced emulsion reactions at 160A GeV and 10.6A GeV, respectively. The predictions of a Monte Carlo code VENUS [13] for the ^{208}Pb data are also included.

Ion	Energy (A GeV)	Events	$\langle N_b \rangle$	$\langle N_g \rangle$	$\langle N_h \rangle$	Ref.
^{208}Pb	160	1034	5.58 ± 0.17	1.96 ± 0.06	7.54 ± 0.23	This work
^{208}Pb	160	1000	0.46	2.16	2.62	VENUS [13]
^{197}Au	10.6	1224	4.98 ± 0.14	2.41 ± 0.06	7.40 ± 0.21	This work

$21 \leqslant Z \leqslant 40$, and $Z > 40$ are less than ± 0.4 charge units (cu), ± 0.5 cu, ± 1.0 cu, ± 2.0 cu, and ± 3.0 cu, respectively. Further details on the charge determination of PF's with $Z > 20$ can be found in Ref. [3].

III. RESULTS ON SLOW PARTICLES

From former studies [12] on the CERN projectiles such as ^{16}O and ^{32}S at (60–200)A GeV, we have learned that the yield of target-associated particles is essentially energy independent, which can be understood simply from geometrical concepts. Here, our objective is to investigate this effect by employing the most massive projectiles accelerated from the SPS and AGS. In Table I, we present the average multiplicities of black $\langle N_b \rangle$, grey $\langle N_g \rangle$, and heavy $\langle N_h \rangle$ target-associated particles emitted in the interactions of the ^{208}Pb ion at 160A GeV and the ^{197}Au ion at 10.6A GeV. It is interesting to find that the average yields of $\langle N_b \rangle$ and $\langle N_g \rangle$ for both the beams are different, but their total $\langle N_h \rangle$ yields are the same. As the target excitation depends on the total yield of the slow particles, $\langle N_h \rangle$, and not on the individual yields of $\langle N_b \rangle$ or $\langle N_g \rangle$ particles, therefore, the target excitation is independent of the projectile energies, though the energies of the ^{208}Pb and ^{197}Au ions differ by a factor of more than 15. In Table I, we also give the predictions of a Monte Carlo code VENUS, version 3.05 [13], on the slow-moving particles produced in the ^{208}Pb-emulsion collisions at 160A GeV. The number of simulated events corresponding to each target in emulsion was generated on the basis of chemical composition of the emulsion detector [11]. The parameter interaction radius r_0 in the code was adjusted to match the nuclear cross section of the generated sample of 1000 events with its corresponding experimental value in emulsion within $\approx 10\%$. It is observed from Table I that the code is unable to predict correctly the average multiplicities of black $\langle N_b \rangle$ and, consequently, of heavy target-related particles. However, the average yield of grey particles, $\langle N_g \rangle$, as predicted by the code agrees very well with the experimental value. From the disagreement between the experimental and the predicted values of $\langle N_b \rangle$ particles, we conclude that the code needs further refinements.

In Figs. 2(a), 2(b), and 2(c), we present the normalized multiplicity distributions of N_b, N_g, and N_h tracks for the ^{208}Pb and ^{197}Au beams. The predictions of a Monte Carlo code VENUS [13] are also shown in these figures by dotted curves. In each of these diagrams, the experimental distributions corresponding to the ^{208}Pb and ^{197}Au projectiles exhibit quite similar behavior. This indicates that the target fragmentation for the ^{208}Pb and ^{197}Au ions is independent of the projectile energy and mass. Once again, the VENUS model explains the results on grey particles quite well, except for a few data points in Fig. 2(b). The model is not efficient enough to produce grey tracks with $N_g > 14$, where the statistics for our experiment is small. However, the code certainly fails to explain the multiplicity distribution of black particles, as one can observe from Fig. 2(a).

IV. RESULTS ON FAST-MOVING PARTICLES

A. Angular measurements and pseudorapidity distributions

The emission angles of the PF's with $Z \geqslant 2$ were measured on a Koristka R-4 microscope using a total magnifica-

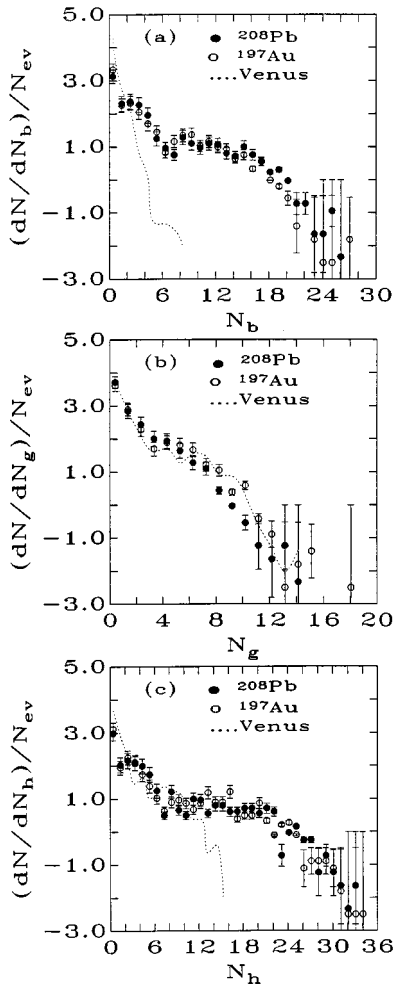

FIG. 2. The normalized multiplicity distributions of the target-associated particles: (a) black tracks N_b, (b) grey tracks N_g, and (c) heavy tracks N_h. The predictions of a Monte Carlo code VENUS [13] are presented by dotted curves.

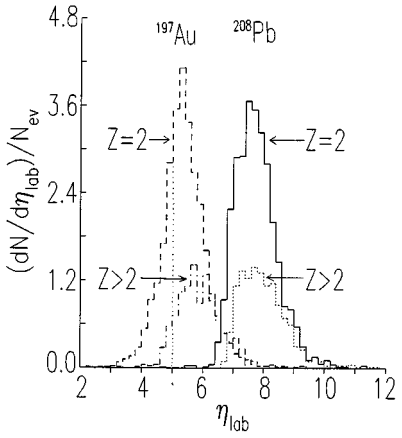

FIG. 3. The normalized pseudorapidity distributions $[(dN/d\eta_{\rm lab})/N_{\rm ev}]$ of the projectile fragments with $Z\geq 2$. For the ^{208}Pb beam: (i) solid-line histogram is for $Z=2$ and (ii) dotted-line histogram is for $Z>2$. For the ^{197}Au data: (iii) dashed-line histogram is for $Z=2$ and (iv) dashed- and dotted-line histogram is for $Z>2$. A vertical dotted line represents the 95% acceptance limit of the ALADIN spectrometer for the detection of lighter fragments with $3\leq Z\leq 5$ [2]. Here, $N_{\rm ev}$ stands for the number of events in a given data set.

tion more than 1000×. The polar angles (θ) of all the PF's were computed from the vector directions of the emitted tracks with respect to a noninteracting primary beam track found in the vicinity of the interaction vertex as described in Ref. [12]. The accuracy in the angular measurements is better than 0.1 mrad for polar angles $\theta\leq 1$ mrad. From the angular measurements, the pseudorapidity ($\eta_{\rm lab}$) of each track in the laboratory frame can be constructed from $\eta_{\rm lab}=-\ln\tan(\theta/2)$. In Fig. 3, we depict the normalized pseudorapidity distribution of 337 events having at least $N_{\rm PF}\geq 4$ of charge $Z\geq 2$ emitted in the ^{208}Pb-induced emulsion collisions at 160*A* GeV. In this figure, we also show the $\eta_{\rm lab}$ distribution of another data set consisting of 378 events of the ^{197}Au ion at 10.6*A* GeV [14] collected under exactly similar experimental conditions. The distributions for the ^{208}Pb and ^{197}Au ions lie in different regions of the pseudorapidity phase space, and thus exhibit an energy-dependent effect of the incident projectile.

The ALADIN Collaboration [2] have studied the fragmentation of the ^{197}Au projectiles interacting with targets of C, Al, and Cu at an incident energy of 600*A* MeV. Because of the strong kinematic focusing effects of the ALADIN spectrometer, the projectile fragments with $Z\geq 6$ were recorded with 100% probability. For lighter fragments with charge $3\leq Z\leq 5$, this probability starts to decline from $\approx$100% for $Z=5$ to about 95% for $Z=3$. For $Z=2$ particles, the detection probability values are $\approx$80% for less violent and $\approx$60% in the case of central ^{197}Au + Al collisions. Since the mean value of charge for several target elements in emulsion is $\langle Z\rangle=13.22$ [11], which corresponds very nearly to the charge number of the Al target, therefore, we are justified in quoting the findings of PF's with $Z\geq 2$ in Ref. [2] for the ^{197}Au + Al collisions. A vertical dotted line as shown in Fig. 3 at $\eta_{\rm lab}=5.0$ corresponds to the 95% acceptance limit quoted by the ALADIN spectrometer array for the detection of lighter fragments of charge $3\leq Z\leq 5$. It is obvious from Fig. 3 that the pseudorapidity distribution of $Z=2$ particles extends to lower values of $\eta_{\rm lab}$ than that of the heavier fragments with $Z\geq 3$, and thus, a substantial number of helium particles would have been missed by the acceptance limit of the ALADIN spectrometer during the recording of the fragmentation of the ^{197}Au beam at 600*A* MeV. But this is not the case for the PF's with $Z\geq 3$. A similar conclusion has also been reported in recent studies using the emulsion detector in Refs. [3] and [4]. However, the discrepancy as reported above in the ALADIN spectrometer can be taken care of by implementing proper corrections, but such corrections cannot be included in the data analysis, which is performed on an event-by-event basis. Thus, this discrepancy would lead to an underestimation of the size of the charge in bound, $Z_{\rm bound}$, in a cluster with $Z\geq 2$ produced in individual events in the analysis of Ref. [2].

B. Average multiplicities of fast-moving particles

In Table II, we display results of the present investigation on the average multiplicities $\langle N_p\rangle$, $\langle N_\alpha\rangle$, and $\langle N_{PF}\rangle$ of the PF's with $Z=1$, $Z=2$, and $Z\geq 3$, respectively, for the ^{208}Pb and ^{197}Au ions. For the sake of a comparison, the results of Cherry *et al.* [4] for the ^{197}Au beam at 10.6*A* GeV are also given in Table II. For the ^{197}Au data, there is an excellent agreement between our results and that of Ref. [4]. The number of singly charged PF's, N_p, can be obtained from the charge conservation. In an individual event, it represents the number of emitted projectile protons:

$$N_p=Z_{\rm beam}-Z_{\rm bound}, \tag{1}$$

where $Z_{\rm beam}$ denotes the incident beam charge. The bound charge is given by

$$Z_{\rm bound}=\sum_{Z\geq 2} Zn(Z), \tag{2}$$

where $n(Z)$ is the multiplicity of the projectile fragments with $Z\geq 2$. This quantity is a measure of the bound charge in

TABLE II. The average multiplicity of projectile fragments with $Z=1$, $Z=2$, and $Z\geq 3$ emitted in the ^{208}Pb- and ^{197}Au-induced emulsion reactions at 160*A* GeV and 10.6*A* GeV, respectively.

Beam	Energy (*A* GeV)	$\langle N_p\rangle$	$\langle N_\alpha\rangle$	$\langle N_{PF}\rangle$	Ref.
^{208}Pb	160	33.22±1.03	3.32±0.10	1.76±0.06	This work
^{197}Au	10.6	28.48±0.81	4.63±0.13	2.01±0.06	This work
^{197}Au	10.6	–	4.53±0.13	1.91±0.06	Cherry *et al.* [4]

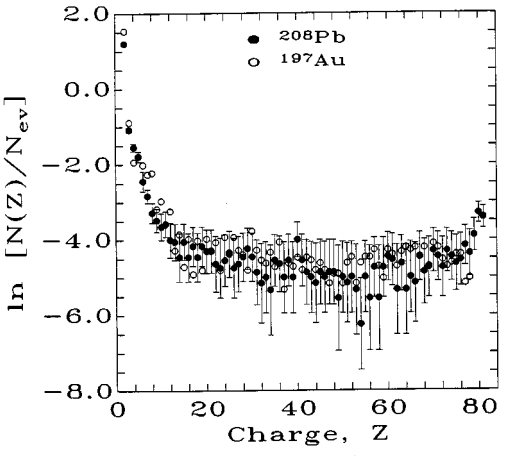

FIG. 4. The normalized distribution ln $[N(Z)/N_{ev}]$ of relative abundances of the PF's with $Z \geq 2$ emitted in (i) ^{208}Pb-emulsion interactions (solid circles) and (ii) ^{197}Au-emulsion collisions (open circles). Errors are plotted only for the ^{208}Pb data for the sake of clarity. The magnitude of error in each data point of the ^{197}Au data is almost of the same order as in the ^{208}Pb data. Here, N_{ev} stands for the number of events in a given data set.

a cluster with $Z \geq 2$ and is complementary to the number of projectile protons [3,14]. One may observe from Table II that the emission of PF's with charge $Z=2$ and $Z \geq 3$ from the ^{208}Pb beam at 160*A* GeV is lower than that for the ^{197}Au beam at 10.6*A* GeV. Consequently, this decrement of the fragment yield for the ^{208}Pb beam of much higher energy will lead to a higher emission of the proton yield for the ^{197}Au data of lower energy. However, the differences in the $\langle N_\alpha \rangle$ and $\langle N_{PF} \rangle$ values for the two samples may be due to a limited statistics or to an energy effect of the incident projectiles.

C. Relative abundances of PF's with $Z \geq 2$

The relative abundances of the PF's with charge $Z \geq 2$ are plotted in Fig. 4 for the data samples of the ^{208}Pb and ^{197}Au beams. Each distribution has a stronger peak for the lighter charges between $2 \leq Z \leq 6$. Both the distributions are quite similar in nature. The relative abundance of the PF's with $Z=2$ is slightly lower for the ^{208}Pb data as compared to the ^{197}Au data. At higher energy, the emission of helium particles seems to be smaller. For the heavier charges ($Z \geq 7$), within errors bars, their relative abundances are almost the same (for the sake of clarity, errors are plotted only for the ^{208}Pb data). It is interesting to find that both data sets (^{208}Pb and ^{197}Au) do not give any evidence of the occurrence of binary fission in the charge range of $35 \leq Z \leq 45$, although a significant enhancement of the fission events was observed at lower energies with the ^{197}Au projectile, as reported in Ref. [4]. Thus, we do not find significant numbers of binary fission events with the ^{208}Pb and ^{197}Au projectiles obtained from the CERN SPS and BNL AGS, respectively. A similar conclusion is also reported by Cherry *et al.* in Ref. [4] for the ^{197}Au beam at 10.6*A* GeV.

D. Correlation between N_α and N_{PF}

Broad characteristics of the projectile fragmentation can be explored through the correlation between the multiplicity of helium particles, N_α, and heavier fragments, N_{PF}. Such a correlation is given in Table III for the ^{208}Pb data. From Table II, one can notice that the number of pure central interactions, in which the projectile has disintegrated completely into singly charged fragments with no emission of heavier fragments, is very small (1.2%) at the CERN energy. More than 20% of the events have $N_\alpha=0$ and $N_{PF}=1$. Only 2.5% of the total number of interactions is found with $N_{PF} \geq 5$ and $0 \leq N_\alpha \leq 10$. On the other hand, only 2.1% of the total number of collisions is observed with $N_{PF}<5$ and $N_\alpha>10$. No event is observed with $N_{PF} \geq 5$ and $N_\alpha>10$. The maximum number of helium fragments observed is $N_\alpha=15$. The maximum number of fragments with $Z \geq 3$ in our sample is $N_{PF}=7$ and that of fragments with $Z \geq 2$ is $N_\alpha + N_{PF}=16$.

TABLE III. Characteristics of projectile fragmentation of the ^{208}Pb beam through a correlation between the number of helium particles, N_α, and the number of heavy fragments, N_{PF}, with $Z \geq 3$.

	Events with different numbers of N_{PF} and N_α							
N_α	$N_{PF}=0$	1	2	3	4	5	6	7
0	12	231	20	3	1	0	0	0
1	8	61	26	6	2	0	0	0
2	14	51	22	17	3	2	1	0
3	9	38	26	14	9	3	1	0
4	7	32	36	26	10	5	1	0
5	4	19	28	26	13	6	1	1
6	3	18	21	13	11	1	0	0
7	3	13	20	18	10	1	1	0
8	1	9	11	14	4	0	0	0
9	4	8	8	7	2	0	1	0
10	1	2	5	3	3	1	0	0
11	0	4	7	3	1	0	0	0
12	0	2	1	1	0	0	0	0
13	1	0	1	0	0	0	0	0
14	0	0	0	0	0	0	0	0
15	0	1	0	0	0	0	0	0

E. Correlation between Z_{max} and Z_{bound}

Before we discuss the correlation between Z_{max} and Z_{bound}, a few comments regarding Z_{bound} may be in order. The parameter Z_{bound}, which was employed by Hubele *et al.* in Ref. [2], is related to the size of the projectile spectator as discussed in Sec. IV B. The energy deposited in a given collision can also be explored through Z_{bound} and it gives a direct measure of the impact parameter of collision [2,3,14].

The maximum charge in each collision, Z_{max}, provides useful information on the exit channel of that collision. Figure 5(a) shows a scatter plot of the correlation between Z_{max} and Z_{bound} for individual events of the ^{208}Pb data. In peripheral collisions, the largest fragment contains most of the total bound charge and in such reactions Z_{max} may be identified as the heavy residue of the beam nucleus after the evaporation. For the central events, we observe that Z_{max} becomes a smaller fraction of Z_{bound}. By definition, Z_{bound} is always larger than or equal to Z_{max}, with the result that most of the data points are situated below the diagonal, which is

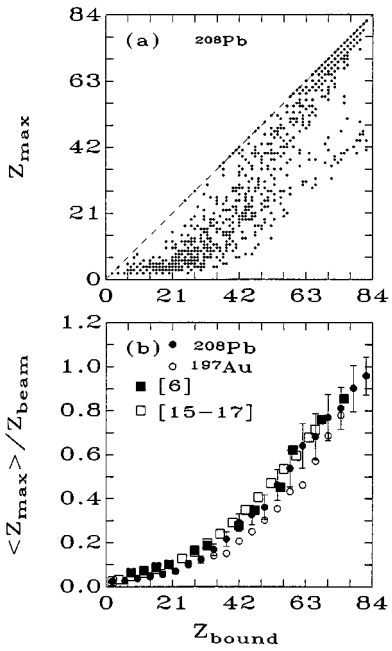

FIG. 5. (a) A scatter plot between the correlation of largest charge Z_{max} and Z_{bound} in individual events of ^{208}Pb at 160*A* GeV. The diagonal is shown by a solid line. (b) A comparison between $\langle Z_{max}\rangle/Z_{beam}$ and Z_{bound} for (i) the ^{208}Pb data (solid circles) and (ii) the ^{197}Au data (open circles). The predictions of the statistical model [6] are shown by solid squares and while those of the percolation model [15–17] are represented by open squares. Errors are given for the ^{208}Pb data as explained in the caption of Fig. 4. Magnitudes of errors are almost the same for both data sets.

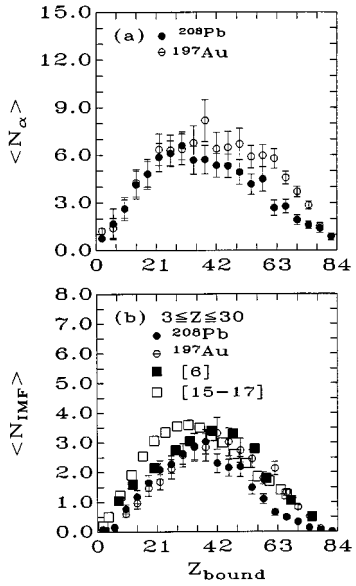

FIG. 6. (a) For the ^{208}Pb and ^{197}Au data samples, $\langle N_\alpha\rangle$ as a function of Z_{bound}. (b) $\langle N_{IMF}\rangle$ as a function of Z_{bound} for the IMF's of charges between $3\leq Z\leq 30$. For the symbols and error bars, refer to the caption of Fig. 5. The symbols used for the model predictions are (i) statistical (solid squares) [6] and (ii) percolation (open squares) [15–17].

shown by a dashed line in Fig. 5(a). As was discussed in Sec. IV C, another notable feature of this figure is that there is no significant evidence for the symmetric fission events occurring at $Z_{max}\approx 41$ and $Z_{bound}\approx 82$. The ^{197}Au data at 10.6*A* GeV also exhibited a similar behavior as was discussed in Refs. [3] and [4].

In Fig. 5(b), we present the variation of $\langle Z_{max}\rangle/Z_{beam}$ as a function of Z_{bound} for the ^{208}Pb data represented by solid circles and that for the ^{197}Au data shown by open circles. To compare these results for the beams of different mass numbers, we have normalized the distribution corresponding to each data set with its respective beam charge Z_{beam}. A sharp rise of $\langle Z_{max}\rangle/Z_{beam}$ as a function of Z_{bound} can be seen from Fig. 5(b) for $Z_{bound}\approx 40-80$. For $Z_{bound}\approx 2-40$, the increment in the parameter $\langle Z_{max}\rangle/Z_{beam}$ is rather slow. It is interesting to find that both heavy beams fragment in a similar manner, irrespective of their primary energies. Smaller values of Z_{bound} correspond to more violent collisions in which a large amount of the projectile energy is consumed in the creation of the shower particles, namely, the pions. Thus, the distribution between $\langle Z_{max}\rangle/Z_{beam}$ and Z_{bound} definitely gives some useful insight into the degree of breakup of the projectile nucleus.

In Ref. [3], we also gave the predictions of statistical [6] and percolation [15–17] models for the ^{197}Au data at 600*A* MeV as discussed in Ref. [2]. For the sake of a comparison, we include in Fig. 5(b) the predictions of statistical [6] and percolation [15–17] models. Within their statistical errors, our results on the ^{197}Au at 10.6*A* GeV and the ^{208}Pb data at 160*A* GeV match reasonably well with the model predictions.

F. Correlation between $\langle N_\alpha\rangle$ or $\langle N_{IMF}\rangle$ and Z_{bound}

In Fig. 6(a), we plot the average multiplicity distributions of helium particles $\langle N_\alpha\rangle$ as a function of Z_{bound} for the ^{208}Pb and ^{197}Au projectiles. Within the statistical errors, these distributions depict a similar behavior for $Z_{bound}\approx 2-50$ and beyond that an apparent departure between them can be noticed for the next four data points. This shows that over limited regions of $Z_{bound}\approx 2-50$ and $Z_{bound}>75$, the breakup process of the two projectiles having different energies is quite similar. However, for the values of $50<Z_{bound}<75$, the projectile fragmentation may depend upon the incident beam energy or the small variation may be due to limited statistics.

Further, we study the emission of intermediate-mass fragments (IMF's) with $3\leq Z\leq 30$. This is presented in Fig. 6(b) through a plot of $\langle N_{IMF}\rangle$ and Z_{bound} for the ^{208}Pb and ^{197}Au ions. As in Fig. 6(a), the $\langle N_{IMF}\rangle$ distributions for the two ions are independent of energy for $Z_{bound}=2-50$ and $Z_{bound}>75$, and for $50<Z_{bound}<75$, the distributions show deviations from one another. For $50<Z_{bound}<75$, the average yield $\langle N_{IMF}\rangle$ of lower energy ^{197}Au ion is larger than that of much higher energy ^{208}Pb ion. This difference between the average multiplicities of $\langle N_\alpha\rangle$ and $\langle N_{IMF}\rangle$ for the two ions may be attributed to limited statistics or to an energy effect. Of course, the so-called ''rise and fall'' of the multifragment emission is clearly observed in the present investigation. In Fig. 6(b), we compare the experimental results ($\langle N_{IMF}\rangle$ versus Z_{bound}) with the predictions of statistical [6] and percolation [15–17] models as was discussed in Ref.

[3]. Our results are better explained by the predictions of the statistical model [6] rather than those of the percolation model [15–17].

V. CHARGED FRAGMENT ASYMMETRIES

In order to facilitate a comparison between the breakup processes of different samples, we now investigate the two-body asymmetries between two or three largest fragments with $Z \geqslant 2$ emitted in individual events. We define the two-body relative asymmetry $R_{\rm as}$ between the first largest $Z_{\rm max1}$ and second largest $Z_{\rm max2}$ charges [2,3] in an event as

$$R_{\rm as}=\frac{Z_{\rm max1}-Z_{\rm max2}}{Z_{\rm max1}+Z_{\rm max2}}. \tag{3}$$

Similarly, another two-body relative asymmetry $R_{\rm as1}$ between the second largest $Z_{\rm max2}$ and third largest $Z_{\rm max3}$ charges [2,3] in an event is defined as

$$R_{\rm as1}=\frac{Z_{\rm max2}-Z_{\rm max3}}{Z_{\rm max2}+Z_{\rm max3}}. \tag{4}$$

For the analysis of two-body asymmetries given by Eq. (3) and (4), we selected the events with at least two and three fragments of $Z \geqslant 2$, respectively. In Fig. 7(a), we plot a variation between $\langle R_{\rm as}\rangle$ and $Z_{\rm bound}$ for the ^{208}Pb and ^{197}Au data. The two-body asymmetry $\langle R_{\rm as}\rangle$ variation is quite similar for both the data samples. Except for the two last data points of the ^{208}Pb ion, this parameter $\langle R_{\rm as}\rangle$ declines monotonically from its maximum value ≈ 0.8 to almost zero as one approaches from extremely peripheral toward more violent collisions. The plot between $\langle R_{\rm as1}\rangle$ and $Z_{\rm bound}$ is shown in Fig. 7(b). For $Z_{\rm bound}<46$, $\langle R_{\rm as1}\rangle$ rises linearly with $Z_{\rm bound}$, except for one data point at $Z_{\rm bound}=4$. For $Z_{\rm bound}>46$, this parameter remains almost constant at $\langle {\rm as1}\rangle \approx 0.25$. Again, it is observed from Fig. 7(b) that for the ^{208}Pb and ^{197}Au projectiles of quite different energies, the breakup process is almost identical. For the comparison between the present experiment and the model predictions on two-body asymmetries, we have also presented in Figs. 7(a) and 7(b) the outcomes of the statistical [6] and percolation [15–17] simulations. Our experimental results corroborate with the model predictions.

We now investigate the breakup process in a more qualitative manner through another parameter known as the three-body asymmetry. Three-body asymmetry [2] is defined as

$$R_{\rm as2}=\frac{\sqrt{(DFA)^2+(DFB)^2+(DFC)^2}}{\sqrt{6}\langle Z\rangle}, \tag{5}$$

where

$$DFA=Z_{\rm max1}-\langle Z\rangle,$$

$$DFB=Z_{\rm max2}-\langle Z\rangle,$$

$$DFC=Z_{\rm max3}-\langle Z\rangle,$$

$$\langle Z\rangle=\tfrac{1}{3}(Z_{\rm max1}+Z_{\rm max2}+Z_{\rm max3}). \tag{6}$$

The parameter $R_{\rm as2}$ has a maximum near unity when there is heavy residue of the projectile spectator and has a zero value when three projectile fragments of equal size are emitted in the collision. In Fig. 7(c), we plot a graph between $\langle R_{\rm as2}\rangle$ and $Z_{\rm bound}$ for events with at least three fragments with $Z \geqslant 2$. The parameter $\langle R_{\rm as2}\rangle$ rises almost linearly with enhancing value of $Z_{\rm bound}$. These distributions exhibit an almost identical behavior, which, once again, leads to an energy independent effect of the breakup mechanism. The maximum value of $\langle R_{\rm as2}\rangle \approx 1$ for the $Z_{\rm bound}$ value very near to the individual beam charge. The minimum value of $\langle R_{as2}\rangle \approx 0$ at $Z_{\rm bound}\approx 9$. This indicates that in our samples of the ^{208}Pb and ^{197}Au beams, some of the events are always accompanied by the emission of three fragments of equal size, $Z=3$. For the sake of clarity, errors are plotted only for the ^{208}Pb data in Figs. 7(a), 7(b), and 7(c). The results of the three-body asymmetries in Fig. 7(c) are also compared with the predictions of the statistical [6] and percolation [15–17] models and they agree reasonably well [6,15–17].

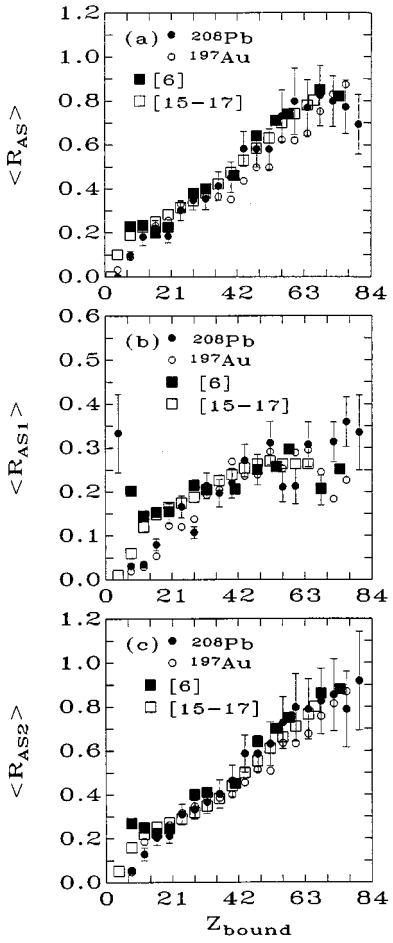

FIG. 7. For the ^{208}Pb and ^{197}Au data samples: (a) A plot of $\langle R_{\rm as}\rangle$ versus $Z_{\rm bound}$, (b) $\langle R_{\rm as1}\rangle$ versus $Z_{\rm bound}$, and (c) $\langle R_{\rm as2}\rangle$ versus $Z_{\rm bound}$. For the definitions of charged particle asymmetries $\langle R_{\rm as}\rangle$, $\langle R_{\rm as1}\rangle$, and $\langle R_{\rm as2}\rangle$; see Sec. V in text. For the symbols and error bars in these figures, refer to the caption of Fig. 5. The symbols used for the model predictions are (i) statistical (solid squares) [6] and (ii) percolation (open squares) [15–17].

VI. CHARGED FRAGMENT MOMENTS

It has been suggested by Campi [16] that the method of conditional moments of the PF's provides a powerful tool to

discriminate between different fragmentation mechanisms. A power law has already been observed in the ^{197}Au data [3,18] and has also been predicted in the clustering size distribution using the percolation models [15–17]. There is no reason that it should not be observed in ^{208}Pb-emulsion collisions at 160*A* GeV. Following Campi's [16] suggestion, we investigated the ith moments of the charge distribution of the n PF's using an event-by-event based analysis:

$$S_i = \sum_{j=1}^{n-1} Z_j^i n_j , \tag{7}$$

where the sum is extended over all the fragments except the largest fragment $Z_{\max 1}$, which is being considered as the percolating cluster. n_j is the multiplicity of different fragments in a given event. The sum in Eq. (7) is computed over all the fragments excluding the heaviest one produced in an event and is normalized by the beam charge Z_{beam}. Exclusion of the largest fragment [16] is done in analogy with the liquid condensation and the percolation cluster and percolation phase transitions. The zero order moment [16] is obtained by putting $i=0$ in Eq. (7):

$$S_0 = \sum_{j=1}^{n-1} n_j . \tag{8}$$

A variation of zero order moment S_0 with Z_{bound} is shown in Fig. 8(a). In order to obtain a better insight into the shape of the distribution of fragment sizes, we examine a combination of the moments S_2, S_0, and S_1. The conditional moment γ_2 is defined as

$$\langle \gamma_2 \rangle = \frac{S_2 S_0}{S_1^2}. \tag{9}$$

In Fig. 8(b), we plot a variation of $\langle \gamma_2 \rangle$ as a function of Z_{bound} for those events with at least two PF's with $Z \geqslant 2$. Moreover, we excluded the singly charged projectile fragments in this analysis. The value of $\langle \gamma_2 \rangle$ increases rather slowly in the range of $2 \leqslant Z_{\text{bound}} < 50$. The maximum value of $\langle \gamma_2 \rangle \approx 1.4$ at $Z_{\text{bound}} \approx 50$, and then decreases for $Z_{\text{bound}} > 50$. Some fluctuations in $\langle \gamma_2 \rangle$ can be seen in this region for the ^{197}Au data. For the lower values of $Z_{\text{bound}} \leqslant 14$, $\langle \gamma_2 \rangle = 1$, and this portion of the graph corresponds to the subsample of events in which the projectile fragments of the same size are emitted. In this subsample, there are two categories of events: One category is with lighter evaporated fragments (after excluding the largest charge) and the other one is with fragments emitted during the total disassembly of the nuclear system. A large value of $\langle \gamma_2 \rangle \approx 1.4$ indicates that the charges in the events are widely distributed. For an infinite nuclear system, the scaling theory of critical phenomena predicts that at the critical point γ_2 diverges at a rate that depends on the critical indices of the phase transition [16]. For a finite nuclear system, γ_2 is predicted to show a smooth behavior [16]. From Fig. 8(b), roughly a smooth increase of $\langle \gamma_2 \rangle$ up to $Z_{\text{bound}} \approx 50$ for the ^{208}Pb data and up to $Z_{\text{bound}} \approx 60$ for the ^{197}Au sample, and then a decrease in their $\langle \gamma_2 \rangle$ values for higher values of Z_{bound} can be noticed. In each case, a broad peak rather than a singularity is due to the finite size of the nuclear system.

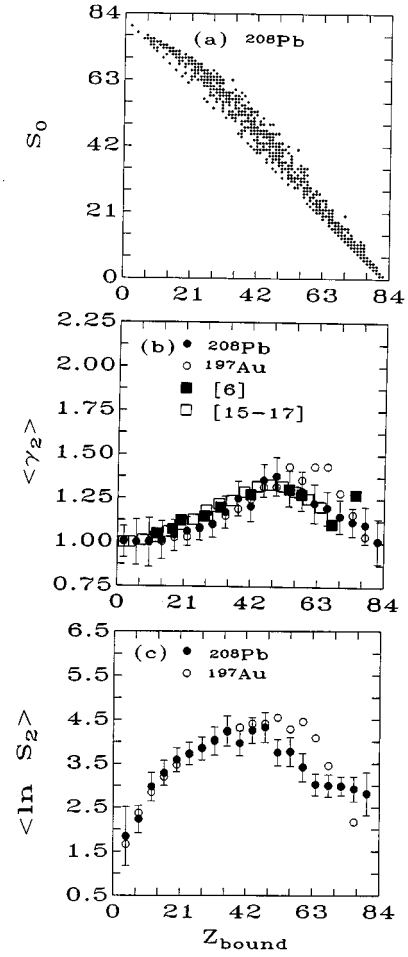

FIG. 8. (a) Correlation between S_0 and Z_{bound} for the ^{208}Pb data at 160*A* GeV. For the ^{208}Pb and ^{197}Au data samples: (b) $\langle \gamma_2 \rangle$ versus Z_{bound} and (c) $\langle \ln S_2 \rangle$ versus Z_{bound}. For the symbols and error bars in (b) and (c), refer to the caption of Fig. 5. The symbols used for the model predictions are (i) statistical (solid squares) [6] and (ii) percolation (open squares) [15–17].

The predictions of the statistical [6] and percolation [15–17] models, as discussed in Ref. [3], are also included in Fig. 8(b). One may notice from Fig. 8(b) that our experimental results on $\langle \gamma_2 \rangle$ vs Z_{bound} are in agreement with the model predictions [6,15–17].

The coexistence of liquid-vapor phase [16] can also be explored by studying a variation of another second conditional moment S_2 as a function of Z_{bound} or the reduced multiplicity of the projectile fragments emitted in an event. In Fig. 8(c), we plot a graph between $\langle \ln S_2 \rangle$ and Z_{bound} for the ^{208}Pb and ^{197}Au beams. In the analysis of Fig. 8(c), singly charged projectile fragments have been excluded. Within the statistical errors, both the distributions show a similar behavior. As discussed above in Fig. 8(b), each distribution has a broad peak in place of a singularity, which is due to the finite size of the nuclear systems employed in this investigation.

VII. CONCLUSIONS

In the present experiment, we have studied, for the first time, the properties of the target- and projectile-associated

particles emitted in interactions of the ^{208}Pb ions accelerated at an energy of 160*A* GeV from the CERN SPS. The results are compared with another sample of the ^{197}Au ions at 10.6*A* GeV obtained from the BNL AGS [3]. From their comparison, the following important conclusions can be summarized.

(i) The average multiplicities of the black $\langle N_b \rangle$ and grey $\langle N_g \rangle$ particles are different for the ^{208}Pb and ^{197}Au projectiles (Table I), but not the average multiplicities of heavy tracks, $\langle N_h \rangle$. The latter fact indicates that the target excitation does not seem to depend either on the beam energy or on its mass. The behavior of the normalized multiplicity distributions of the N_b, N_g, and N_h particles also shows an energy independent effect: See, for example, Figs. 2(a), 2(b), and 2(c) in Sec. III. The Monte Carlo code VENUS [13] explains, in a reasonably good manner, the results on the average multiplicity $\langle N_g \rangle$ of grey particles (Table I) and their normalized multiplicity distributions $[(dN/dN_g)/N_{\rm ev}]$ as shown by a dotted curve in Fig. 2(b), where $N_{\rm ev}$ represents the number of events in a given data sample. However, the code is not adequately efficient to explain the average yields of black $\langle N_b \rangle$ and heavy $\langle N_h \rangle$ target-related particles (Table I). This is also valid for the normalized multiplicity distributions of N_b and heavy N_h particles as shown by dotted curves in Figs. 2(a) and 2(c).

(ii) The normalized pseudorapidity $\eta_{\rm lab}$ distributions of helium and heavier projectile fragments are observed to be dependent upon the incident beam energy, and thus found to lie in different regions of the pseudorapidity phase space. Because of the 95% acceptance limit in the ALADIN spectrometer, a substantial number of projectile helium particles has been missed in Ref. [2]. A recent study by Cherry *et al.* in Ref. [4] supports our results on the ^{197}Au beam at 10.6*A* GeV.

(iii) The average multiplicities of the fast-moving projectile particles such as $\langle N_\alpha \rangle$, $\langle N_{PF} \rangle$, and $\langle N_p \rangle$ seem to depend upon the mass and energy of the incident projectile (Table II). This effect could be due to a limited statistics employed in this work. The multifragment emission is a dominant reaction channel when investigated from the distributions of $\langle N_\alpha \rangle$ and $\langle N_{\rm IMF} \rangle$ as a function of $Z_{\rm bound}$. These distributions are peaked at $Z_{\rm bound} \approx 30$–40 and ≈ 42 for the ^{207}Pb and ^{197}Au projectiles, respectively. For $Z_{\rm bound} \approx 2$–50 and $Z_{\rm bound} > 75$, the distributions almost overlap within their statistical errors and some deviations are observed in the range of $50 < Z_{\rm bound} < 75$. The partial universal behavior of the $\langle N_\alpha \rangle$ or $\langle N_{\rm IMF} \rangle$ for $Z_{\rm bound} \approx 2$–50 and $Z_{\rm bound} > 75$ suggests that the excitation energy of the projectile nucleus is independent of the beam energy and its mass.

(iv) Two- and three-body asymmetries are explored through the distributions of $\langle R_{\rm as} \rangle$, $\langle R_{\rm as1} \rangle$, and $\langle R_{\rm as2} \rangle$ as a function of $Z_{\rm bound}$ for the ^{208}Pb and ^{197}Au ions. Within statistical errors, the distributions show almost similar behavior, which indicates that the breakup mechanism for both data sets is almost identical. From these observations, once again, we conclude that the excitation of the projectile nucleus seems be to energy independent, which is also predicted by the statistical [6] and percolation [15–17] models with low energy ^{197}Au data in Refs. [2,3].

(v) A comparison of the conditional moments such as $\langle \gamma_2 \rangle$ for the ^{208}Pb and ^{197}Au beams also proves that the breakup mechanisms involved for the projectile fragments are nearly the same [Fig. 8(b)]. A broad peak rather than a singularity in Fig. 8(b) for the ^{208}Pb and ^{197}Au data samples indicates that the nuclear systems employed in the present investigation have finite size. A similar inference is also obtained from Fig. 8(c), where we have plotted $\langle \ln S_2 \rangle$ as a function of $Z_{\rm bound}$ for the ^{208}Pb and ^{197}Au data sets. The experimental results of the conditional moments $\langle \gamma_2 \rangle$ versus $Z_{\rm bound}$ agree quite well with the predictions of statistical [6] and percolation [15–17] models.

ACKNOWLEDGMENTS

We are thankful to the CERN SPS technical staff in an excellent exposure and to Prof. G. Romano for the development of our emulsion stacks. This research work was partially supported by the U.S. DOE and partially by the Research Foundation, SUNY at Buffalo.

[1] Y. D. Kim *et al.*, Phys. Rev. Lett. **63**, 494 (1989); Blumenfeld *et al., ibid.* **66**, 576 (1991); E. Piasecki *et al., ibid.* **66**, 1291 (1991); D. R. Bowman *et al., ibid.* **67**, 1527 (1991).

[2] C. A. Ogilvie *et al.*, Phys. Rev. Lett. **67**, 1214 (1991); K. Hagel *et al., ibid.* **68**, 2141 (1992); J. Hubele *et al.*, Z. Phys. **340**, 263 (1991); J. Hubele *et al.*, Phys. Rev. C **46**, R1577 (1992); P. Kreutz *et al.*, Nucl. Phys. **A556**, 672 (1993).

[3] P. L. Jain, G. Singh, and A. Mukhopadhyay, Phys. Rev. C **50**, 1085 (1994); G. Singh and P. L. Jain, *ibid.* **49**, 3320 (1994).

[4] M. L. Cherry *et al.*, Phys. Rev. C **52**, 2652 (1995); C. J. Waddington, Int. J. Phys. E **2**, 739 (1993).

[5] D. G. d'Enterria *et al.*, Phys. Rev. C **52**, 3179 (1995); W. Heinrich, E. Winkel, G. Rusch, J. Dreute, and B. Wiegel, in Proceedings of the Interactions Workshop XXII, 1994 (unpublished).

[6] D. H. E. Gross, Rep. Prog. Phys. **53**, 605 (1990) and references therein; H. R. Jaqaman and D. H. E. Gross, Nucl. Phys. **A524**, 321 (1991); B. A. Li, A. R. DeAngelis, and D. H. E. Gross, Phys. Lett. B **303**, 225 (1993); D. H. E. Gross, Z. Xia-ze, and X. Shu-an, Phys. Rev. Lett. **56**, 1544 (1986).

[7] H. W. Barz, J. P. Bondorf, R. Donangelo, and H. Schulz, Phys. Lett. **169B**, 318, (1986); J. Bondorf *et al.*, Nucl. Phys. **A444**, 460 (1985).

[8] G. F. Bertsch and S. Das Gupta, Phys. Rep. **160**, 189 (1988); H. Stocker and W. Gneiner, Phys. Rep. **137**, 277 (1986); P. Schuck *et al.*, Prog. Part. Nucl. Phys. **22**, 181 (1989); W. Baur, C. K. Gelbke, and S. Pratt, Annu. Rev. Nucl. Part. Sci. **42**, 77 (1992); P. Danielewicz and G. F. Bertsch, Nucl. Phys. **A533**, 712 (1991).

[9] G. Peilert *et al.*, Phys. Rev. C **39**, 1402 (1989); J. Aichelin, Phys. Rep. **202**, 233 (1991).

[10] A. Aranda, C. O. Dorso, V. Furci, and J. A. Lopez, Phys. Rev. Lett. **52**, 3217 (1995); S. Ayik and C. Gregoire, Nucl. Phys. **A513**, 187 (1990); J. Randrup and B. Remaud, *ibid.* **A514**,

339 (1990); Ph. Chomaz, G. F. Burgio, and J. Randrup, Phys. Lett. B **254**, 340 (1991); G. F. Burgio, Ph. Chomaz, and J. Randrup, Nucl. Phys. **A529**, 157 (1991); Phys. Rev. Lett. **69**, 885 (1992).

[11] C. F. Powell, P. H. Fowler, and D. H. Perkins, *The Study of Elementary Particles by the Photographic Method* (Pergamon Press, London, 1959).

[12] P. L. Jain, K. Sengupta, and G. Singh, Phys. Rev. C **44**, 844 (1990).

[13] K. Werner, Phys. Lett. B **208**, 520 (1988).

[14] P. L. Jain, G. Singh, and A. Mukhopadhyay, Phys. Rev. Lett. **74**, 1534 (1995).

[15] W. Bauer, Phys. Rev. C **38**, 1297 (1988); W. Bauer *et al.*, Annu. Rev. Nucl. Sci. **42**, 77 (1992); J. D. Desbois, Nucl. Phys. **A466**, 724 (1987).

[16] X. Campi, J. Phys. A **19**, L917 (1986); Phys. Lett. B **208**, 351 (1988).

[17] D. Stauffer, Phys. Rep. **54**, 1 (1979).

[18] P. L. Jain and G. Singh, Nucl. Phys. **A591**, 711 (1995).